Sensors and Materials, Vol. 33, No. 12 (2021) 4383–4397
MYU Tokyo

S & M 2769

Demonstration of Particle–Substrate Surface Interaction Analysis Based on Brownian Motion and Gravitational Testing

Mao Otake[1,2] and Yoshiaki Ukita[1*]

[1]University of Yamanashi, 4-4-37, Takeda, Kofu, Yamanashi 400-8510, Japan
[2]Research Fellow of Japan Society for the Promotion of Science,
5-3-1 Kojimachi, Chiyoda-ku, Tokyo 102-0083, Japan

(Received September 1, 2021; accepted December 21, 2021)

Keywords: bead-based bioassay, physical adsorption, DLVO theory, Brownian motion, image analysis

In this paper, we propose a simple method for analyzing interface interactions in bead-based bioassay. Although bead-based bioassay enables simple and rapid quantitative evaluation of target substances, non-specific adsorption between the beads or between the beads and a substrate affects the reliability of measurement. Conventional methods for evaluating non-specific adsorption include a method in which a magnetic force or shearing force is applied to beads to prevent non-specific adsorption, but the experimental system is complicated. Therefore, a simpler evaluation method would be useful for carrying out a systematic study to find optimal conditions for the suppression of non-specific adsorption. Therefore, we devised a new adhesion behavior analysis method based on simple force application by gravity and the observation of Brownian motion. The analysis results obtained by the devised method were considered on the basis of DLVO (Derjaguin–Landau–Verwey–Overbeek) theory, which is the adhesion theory of solid surfaces, and the main factors contributing to non-specific adsorption were identified. Furthermore, changes in adhesion behavior with ionic strength, bead size, and reaction time were investigated. The results provide useful information for optimizing the experimental system in bead-based bioassay and are expected to improve the reliability of bioassay.

1. Introduction

Biosensing utilizes the molecular recognition ability of biomolecules to detect target molecules, using the binding of antigens and antibodies, DNAs, and other ligands and receptors by specific reactions.(1) Radioisotopes,(2–4) fluorescent dyes,(5–7) and enzymes(8–10) are used to detect these intermolecular bonds. By labeling a molecule that recognizes and binds to the target molecule with these substances, the amount of the target molecule can be quantified from the radiation or fluorescence intensity or the amount of color development. Microbeads have also long been studied as a labeling material that can detect target molecules easily and quickly.(11–13) Receptor molecules that react with the target molecules are fixed on the surface of the microbeads or the substrate, and the reaction with the target molecules results in the formation of a specific bond between the beads or between the beads and the substrate. The detection and

*Corresponding author: e-mail: yukita@yamanashi.ac.jp
https://doi.org/10.18494/SAM.2021.3613

ISSN 0914-4935

quantitative evaluation of the target molecules can be realized by observing the microbeads bonded to the substrate or the bead aggregates with optical technology or the naked eye. Such bead-based bioassay is characterized in that, by simplifying the washing operation after the reaction with the target molecules, the measurement can be speeded up and the cost of the apparatus can be reduced. In addition, it is possible to perform not only quantitative evaluation but also qualitative evaluation of intermolecular interactions at the same time by applying a magnetic force[12,14] or centrifugal force[15,16] to the beads for measurement of the binding force. Therefore, there is also potential to develop a new molecular analysis method whose principle is different from that of the conventional immunoassay method. However, in the case of bead-based bioassay, the adhesion of beads to the substrate and the aggregation of beads due to non-specific interactions are major problems. The adhesion and aggregation of beads by non-specific interactions increase the background noise, which is expected to reduce the measurement reliability, such as by decreasing the detection sensitivity. For this reason, in the development of bead-based bioassay, trial and error is usually performed to reduce non-specific adhesion. There are two main approaches to suppressing the non-specific adsorption of beads: surface modification and removal of non-specifically adsorbed particles.[17] For example, it is widely known that introducing a molecular chain of polyethylene glycol (PEG) to a substrate suppresses the non-specific adhesion of beads.[12,18,19] However, even when such a method is introduced, trial and error is necessary to find the optimal conditions such as the modification density and the length of the molecular chain to obtain a sufficient effect.[20] To evaluate the effect of such modification, an evaluation system that is similar to an actual assay was constructed, and a magnetic force[12] or a shear force imposed by a fluid[13] was applied to estimate the non-specific interaction. In this method, since it is necessary to construct an experimental system using an electromagnet or a liquid feed pump in every test, the operation becomes complicated and systematic examination is difficult.

Therefore, in this paper, we have developed a method that can analyze the interaction between particles and the surface of a substrate with a simple operation. In addition, we report the results of an attempt to analyze the adhesion phenomenon of beads based on this technology.

2. Materials and Methods

2.1 Preparation of reagents

Dulbecco's phosphate-buffered saline (DPBS) was adjusted to have a concentration of 100 mM and pH 7.2 to 7.4. 2-[4-(2-Hydroxyethyl)-1-piperazinyl] ethane sulfonic acid (HEPES, Dojindo & Co., Ltd., Japan, #344-08231) was dissolved in Milli-Q water (Simplicity UV, Merck Millipore) to 1 M. NaOH (Wako Pure Chemical Industries, Ltd., Japan #198-13765) was dissolved in Milli-Q water to 1 M. NaCl (Nacalai Tesque, Inc., Japan #31320-05) was dissolved in Milli-Q water to 1 M. The pH was adjusted by adding 1 M NaOH solution to the 1 M HEPES solution, and the ionic strength was adjusted by adding 1 M NaCl solution. A HEPES solution with a pH of 6.90 ± 0.05 was prepared by diluting the above mixed solution with Milli-Q water to a HEPES concentration of 10, 25, or 50 mM. The concentration of NaOH required for pH

adjustment was determined from the acid dissociation constant and the final concentration of HEPES based on the Henderson–Hasselbalch formula. Polystyrene beads having a diameter of 3 μm (Polybead Carboxylate 3.0 Micron Micro Spheres (2.5% Solids-Latex), Polysciences #09850-5, PS-COOH) were used as carboxylate microbeads. Similarly, polystyrene beads having a diameter of 3 μm (Polybead Amino 3.0 Micron Micro Spheres (2.5% Solids-Latex, Polysciences #17145-5, PS-NH2) were used as aminate polystyrene beads. We used 1.0526 g/cm^3 for the density of polystyrene beads, which is the value measured in a past study.[16] Each bead suspension was added to a HEPES solution so that the bead concentration was about 5000 particles/μl, then stirred with a vortex. Centrifugation was performed at 1000 g for 10 min, the supernatant was removed, and the HEPES solution was added again. The dispersion medium of the polystyrene beads was completely replaced by repeating the above solvent replacement procedure three times.

2.2 Measurement of zeta potential

A zeta potential analyzer (ELSZ-2000, Otsuka Electronics, Japan) was used to measure the zeta potential. Absolute value measurement was performed for the glass substrate and PS-COOH to estimate the surface potentials of the beads and the substrate in the experimental environment. In addition, titration was performed for isoelectric point measurement of the beads and substrate. In the absolute value measurement, a HEPES buffer adjusted to have an ionic strength of 10 mM and a pH of 6.9 ± 0.5 was used as a dispersion medium for the beads. In the titration measurement, a 10 mM NaCl aqueous solution was used as the dispersion medium for the beads. The beads were suspended by diluting the bead suspension 10000 times with each buffer and the diluted suspension was added to the measuring cell. In the titration measurement, changes in the zeta potential were observed by measuring the pH during the dropwise addition of 0.1 M HCl and 0.1 M NaOH aqueous solutions.

2.3 Construction of observation system

An outline of the observation system is shown in Fig. 1. A slide glass (Matsunami Glass Ind., Ltd., Japan #S2441) was used as the glass substrate to interact with the beads. Sheetlike polydimethylsiloxane (PDMS, SILPOT 184, Dow Corning Toray Co., Ltd., Japan) was used to

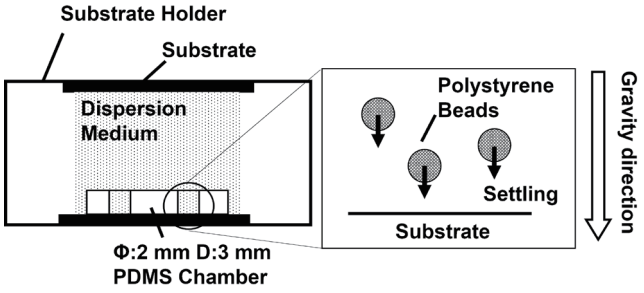

Fig. 1. Schematic of experiment device.

prepare the reaction chamber. The PDMS prepolymer and the cross-linking agent were mixed at a ratio of 10:1 (w/w), and the mixture was poured into a mold. A PDMS sheet having a thickness of 3 mm was prepared by curing the PDMS at 100 °C for 35 min. A 2 mm hole was punched in the PDMS sheet. Then, the PDMS sheet and the glass substrate were ultrasonically cleaned with ethanol and ion-exchanged water for 3 min each, which was followed by drying in a stream of N_2 and attaching the PDMS sheet to the substrate. The glass substrate with the reaction chamber was attached to a self-made substrate holder. After adding 5 µl of HEPES solvent to the chamber, 5 µl of bead suspension was added and mixed by pipetting several times. Then, the inside of the holder was filled with HEPES solution, and the upper surface was sealed with a slide glass as shown in Fig. 1. The sample was photographed using an sCMOS camera (ORCA-Flash 4.0 V2, Hamamatsu Photonics, Japan) connected to an inverted microscope (IX71, OLYMPUS, Japan) and software (HC Image Live 4.2.6, Hamamatsu Photonics, Japan).

2.4 Calculation of bead sedimentation rate

As shown in Fig. 1, the beads in the reaction chamber are estimated to settle at settling speed v and approach the slide glass. From Stokes' equation, the particle settling velocity v is

$$v = \sqrt{\frac{4(\rho_b - \rho_m) g d}{3 \rho_m C_d}}, \tag{1}$$

where ρ_b is the density of beads, ρ_m is the density of solvent, g is gravitational acceleration, d is the particle diameter, and C_d is the drag coefficient of the particle. C_d is estimated using the particle Reynolds number Re^*:

$$C_d = \frac{24}{Re^*}, \tag{2}$$

$$Re^* = \frac{vd}{\eta / \rho_m}, \tag{3}$$

where η is the viscosity of the dispersion medium. By substituting Eqs. (2) and (3) into Eq. (1), the particle settling velocity can be expressed as

$$v = \frac{(\rho_s - \rho_w) g}{18 \eta} d^2. \tag{4}$$

By substituting each physical property value, the settling velocity of the beads dispersed in pure water was obtained as $v \approx 0.29$ µm/s. Since the chamber height is 3 mm, it should take about 172 min for all the beads to reach the substrate surface. Therefore, to sufficiently settle the beads

added to the reaction chamber, the holder enclosing the beads was allowed to stand at room temperature for 3 h.

2.5 Measurement of bead adhesion rate

2.5.1 Adhesion rate measurement by gravity sedimentation method

Observation was performed using an inverted microscope and a 10× objective lens with the beads sufficiently settled and interacting with the substrate. A microscope image of the beads on the surface of the substrate was obtained with an sCMOS camera. After that, the holder was turned upside down so that the beads not adhering to the substrate were separated from the substrate by gravity. The substrate and beads were sufficiently separated by allowing them to stand at room temperature for 3 h in the same manner as in Sect. 2.3, then another microscope image was obtained. Image analysis was performed on the acquired microscope images using ImageJ[21] open-source image processing software and Fiji,[22] which is a plug-in package of ImageJ. The bead adhesion rate was calculated by automatically counting the number of beads before and after separation by image analysis.

2.5.2 Adhesion rate measurement by Brownian motion analysis

During the procedure described in Sect. 2.5.1, a time-lapse movie (20 fps) of the beads on the substrate surface was taken for 5 s. The maximum brightness of the same pixel of the captured moving image was extracted from all frames to generate an image for analysis. The time-lapse video is provided in the supplementary material (URL: https://youtu.be/xTUCc5kNxIo). In the video, beads for which Brownian motion can and cannot be visually confirmed can be observed. The generated averaging image is shown in Fig. 2(a). This image was taken with a 40× objective lens, different from that used in the experimental environment, for visibility. As shown in Fig. 2(a), the beads not attached to the substrate fluctuated as a result of Brownian motion, and their outline became unclear. On the other hand, since the Brownian motion of the beads attached to the substrate was constrained by the interaction with the

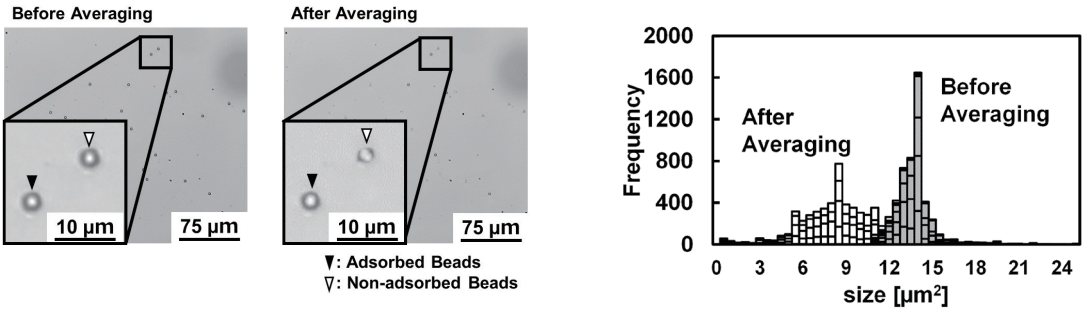

(a) (b)

Fig. 2. Detection of non-adhering particles by image averaging. (a) Particle images before and after image averaging. (b) Histogram of detected particle size.

substrate, a clear image of the beads was obtained. Figure 2(b) shows a histogram of the size of beads detected before and after image averaging for beads existing in the same chamber. Image analysis was performed on the four reaction chambers and the results were integrated. As shown in Fig. 2(b), the detected bead size changed from an average of 31.8 pixels and a standard deviation of 4.9 pixels before averaging the images to an average of 19.1 pixels and a standard deviation of 6.0 pixels after averaging, indicating that the particle size was reduced by about 40% by image processing. From the above, it is possible to identify the adhering/non-adhering state of beads by applying an appropriate threshold. The adhesion rate of the beads was determined by distinguishing between the beads undergoing and not undergoing Brownian motion on the substrate. To evaluate the time change of the bead adhesion rate, the above time-lapse movie filming was performed for 30 min with 1 min intervals immediately after the application of beads, and the adhesion rate at each time was calculated.

2.6 Calculation of potential energy based on DLVO theory

Derjaguin–Landau–Verwey–Overbeek (DLVO) theory is a basic theory for predicting the dispersion/aggregation of colloids.[23] In DLVO theory, the interaction between solid surfaces is estimated by the sum of the potential energies V_a and V_r, where V_a is the potential energy due to the van der Waals force applied by the dipole and V_r is the electrostatic potential energy formed by the adsorption of counterions in the dispersion medium on the solid surface due to surface charging.

The van der Waals potential V_a between the particle and the substrate is calculated as

$$V_a = \frac{-Aa}{6D}, \tag{5}$$

where a is the particle radius and D is the distance between the particle and the substrate. A is the Hamaker constant, which has a different value for each substance; the Hamaker constant of the entire system can be expressed in terms of A_1, A_2, and A_3, the Hamaker constants for the particle material, substrate material, and dispersion solvent, respectively:

$$A = \left(\sqrt{A_1} - \sqrt{A_3}\right)\left(\sqrt{A_2} - \sqrt{A_3}\right). \tag{6}$$

The potential energy due to the electric double layer was calculated as

$$V_r = \pi\varepsilon_0\varepsilon a\left(\psi_1^2 + \psi_2^2\right)\left[\frac{2\psi_1\psi_2}{\psi_1^2 + \psi_2^2}\ln\frac{1+e^{-\kappa D}}{1-e^{-\kappa D}} + \ln\left(1-e^{-2\kappa D}\right)\right], \tag{7}$$

where ε_0 is the permittivity of the vacuum, ε is the relative permittivity of the dispersion solvent, e is the elementary charge, and ψ_1 and ψ_2 are the surface charges of the particles and the

substrate, respectively. In addition, κ^{-1} is the Debye length, representing the thickness of the electric double layer and is calculated as

$$\kappa^{-1} = \sqrt{\frac{\varepsilon_0 \varepsilon kT}{2\rho_\infty e^2}}, \tag{8}$$

where k is the Boltzmann constant, T is the absolute temperature, and ρ_∞ is the number density of counterions present in the bulk solvent. If the ion concentration C [mol/L] is used instead of ρ_∞, the following equation is obtained:

$$\kappa^{-1} = \sqrt{\frac{\varepsilon_0 \varepsilon kT}{2000 N_A C e^2}}, \tag{9}$$

where N_A is Avogadro's number. In addition, the ionic strength is calculated as

$$I = \sum_{I=1} \left(\frac{1}{2} C_i Z_i^2 \right), \tag{10}$$

where Z is the valence of the ionic species. In this experiment, the valences of all the ionic species used are 1, so the ionic strength is calculated as

$$I = \sum_{I=1} \left(\frac{1}{2} C_i Z_i^2 \right) = \frac{1}{2} \left(2C_{\mathrm{NaOH}} + 2C_{\mathrm{NaCl}} \right) = C_{\mathrm{NaOH}} + C_{\mathrm{NaCl}}, \tag{11}$$

where C_{NaOH} is the concentration of NaOH and C_{NaCl} is the concentration of NaCl. From the above, in this experiment, the total concentration of the salt added to the solvent becomes the ionic strength, which is used for the calculation of the Debye length.

From the above, the total potential energy V_t acting between the solid particles and the solid substrate based on DLVO theory can be expressed as

$$V_t = V_a + V_r = \frac{-Aa}{6D} + \pi \varepsilon_0 \varepsilon a \left(\psi_1^2 + \psi_2^2 \right) \left\{ \frac{2\psi_1 \psi_2}{\psi_1^2 + \psi_2^2} \ln \frac{1 + e^{-\kappa D}}{1 - e^{-\kappa D}} + \ln \left(1 - e^{-2\kappa D} \right) \right\}. \tag{12}$$

The force F acting between the particles and the substrate can be expressed as

$$F = -\frac{dV_t}{dD} = -\left(\frac{dV_a}{dD} + \frac{dV_r}{dD} \right) = \frac{-AR}{6D^2} - \pi \varepsilon_r \varepsilon_0 a \left(\psi_1^2 + \psi_2^2 \right) \left(\frac{2\psi_1 \psi_2}{\psi_1^2 + \psi_2^2} \cdot \frac{-2\kappa e^{-\kappa D}}{1 - e^{-2\kappa D}} + \frac{2\kappa e^{-2\kappa D}}{1 - e^{-2\kappa D}} \right), \tag{13}$$

by differentiating V_t with respect to the distance D between the particles and the substrate.

3. Results and Discussion

3.1 Zeta potential measurement

The zeta potentials obtained by absolute value measurement were −39.45 ± 1.63 mV for the glass substrate and −74.98 ± 0.42 mV for PS-COOH. Figure 3 shows the results of zeta potential measurement by titration. From Fig. 3, the isoelectric points of the surface of PS-COOH and the surface of the glass substrate are 4.18 and 4.04, respectively. Therefore, the electrostatic interaction is considered to act in the repulsive direction because the functional groups on the surface of both the beads and the substrate are deprotonated and negatively charged at around pH 6.9, which is the experimental pH.

3.2 Analysis of effect of ionic strength by gravity settling method

The adhesion rate was measured using DPBS, which is a phosphate buffer used in general bioassay, as a dispersion medium. Figure 4 shows the bead adhesion rates obtained by the gravity settling method when DPBS and ultrapure water were used as the dispersion medium. In the case of DPBS, the bead adhesion rate is almost 100%, and in the case of ultrapure water, the bead adhesion rate is almost 0%. These results can be explained by DLVO theory as described later. Thus, the gravity settling method can easily provide a quantitative index for the physical interaction at the nanometer-scale interface.

Figure 5 shows the measured adhesion rates of beads in HEPES buffer. The use of HEPES has the advantage that its own ionic strength is low and can be adjusted independently of pH by adding a salt. Figure 5 shows that the bead adhesion rate increased in a sigmoid curve as the ionic strength increased. It was found that the adhesion rate reached almost 100% at an ionic strength of about 30 mM. Furthermore, no significant correlation was observed between the HEPES concentration and the bead adhesion rate. Therefore, the increase or decrease in ionic strength due to NaOH and NaCl in the solvent had a dominant effect on the adhesion rate of beads. HEPES comprises zwitterions in aqueous solution, and it remains contested whether

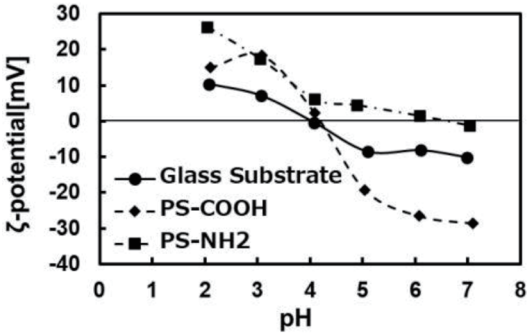

Fig. 3. Results of zeta potential measurement by titration.

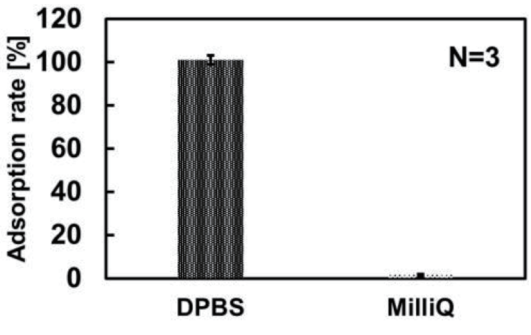

Fig. 4. Comparison of bead adhesion rate when DPBS and ultrapure water are used as the dispersion medium.

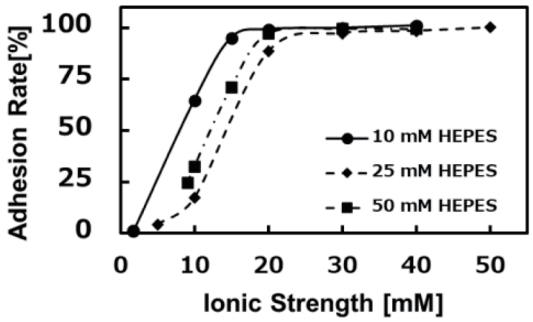

Fig. 5. Relationship between ionic strength of HEPES solution (pH 6.8) and bead adhesion rate.

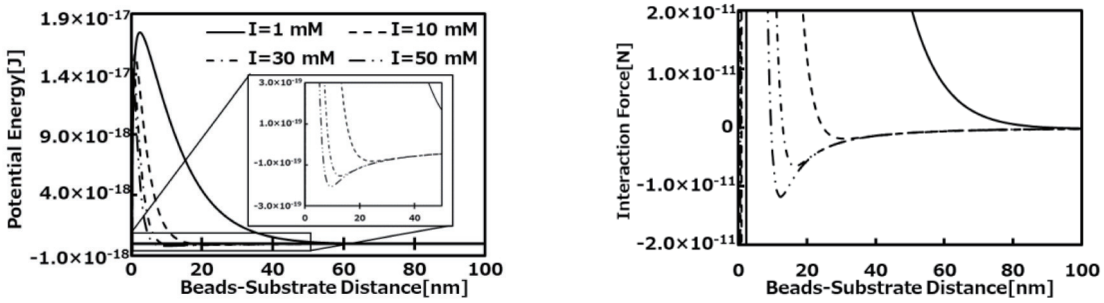

(a) (b)

Fig. 6. Simulation of bead adhesion behavior based on DLVO theory. (a) Potential energy curve. (b) Interaction force curve.

zwitterions affect the ionic strength in the solvent.[24] In this experiment, no significant effect of the HEPES concentration on the bead adhesion rate was observed; thus, it can be concluded that the effect of the ionic strength of HEPES on bead adhesion is limited.

Figures 6(a) and 6(b) show the potential energy between the beads and the substrate calculated on the basis of DLVO theory and the force acting between the beads and the substrate, respectively. It can be seen from Fig. 6(b) that when the ionic strength I = 1 mM, the bead–substrate repulsive force extends farthest. According to DLVO theory, when the ionic strength of the dispersion medium is high, the solid surface is electrically neutralized and the van der Waals attraction becomes dominant. On the other hand, when the ionic strength of the dispersion medium is low, the counterions that neutralize the surface potential decrease in number, so the distance over which the surface potential has an effect increases. In the above case, when the particles approach the surface from a distance, the electrical repulsive force becomes dominant before the attractive force due to the van der Waals force. As can be seen from Figs. 6(a) and 6(b), when the ionic strength increases, an attractive force acts between the bead and the substrate due to the local minimum value being before the local maximum of the potential curve. Therefore, it is considered that the adhesion rate in this experiment increased because the ionic strength increased, and the van der Waals force became dominant. As described above, on the basis of DLVO theory, the non-specific adhesion of beads is considered to be due to the influence of van der Waals attraction.

3.3 Effect of gravitational potential on adhesion rate

The discussion so far has not considered the gravitational potential. To investigate the effect of gravitational potential, we measured the adhesion rate of beads with particle sizes of 3, 10, and 20 μm, the results of which are shown in Fig. 7. Beads with a diameter of 3 μm have the lowest adhesion rate to the substrate at all ionic strengths. In particular, there is almost no adhesion to the substrate at a low ionic strength of 1.8 or 2 mM. On the other hand, the adhesion rates of the beads of 10 and 20 μm diameter at these low ionic strengths were about 50–60 and 97–100%, respectively. That is, the larger the particle size, the more beads are adhered to the substrate, even at a low ionic strength. The Van der Waals force and electrical repulsion are proportional to the particle radius, while the particle's own weight increases in proportion to the cube of the particle radius and thus increases more rapidly than the strength of the interaction. Therefore, it is possible that the DLVO potential barrier was overcome by a change in the curvature of the interface or the weight of the beads due to an increase in radius.

Figure 8 shows the calculated potential energy at the ionic strength I = 10 mM and the interaction force between the beads and the substrate. The potential energy calculation did not take into account the energy due to gravity acting on the particles. For the surface potential used in the calculation, the absolute value of the zeta potential measured in Sect. 3.1 was used.

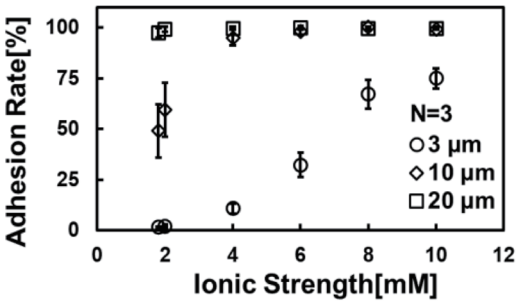

Fig. 7. Effect of bead particle diameter on adhesion rate.

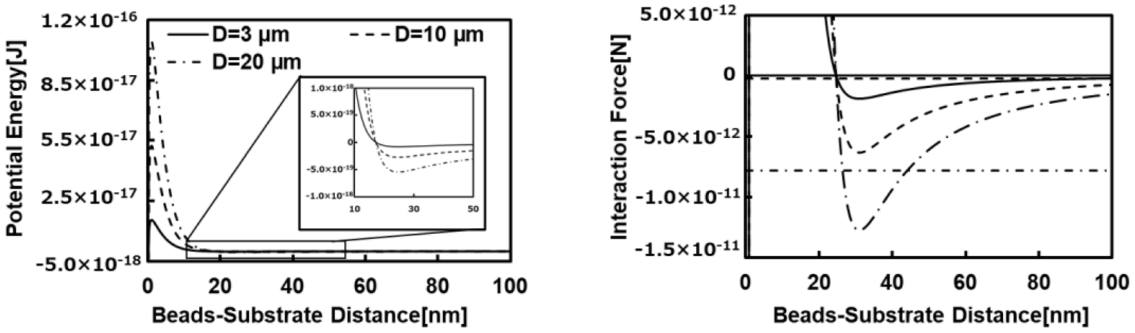

(a) (b)

Fig. 8. Bead diameter and potential energy. (a) Potential energy curves. (b) Comparison of interaction force curve and gravity. The horizontal lines indicate the sedimentation force acting on the beads by gravity in a solvent with a specific density of 1.

Therefore, in this section it is assumed that the zeta potentials of the 10 and 20 μm particles are the same as those of the 3 μm particles. The horizontal lines in Fig. 8(b) show the sedimentation force acting on the beads in the solvent having a specific gravity of 1, where the solid line, broken line, and dot-dashed line represent the magnitude of gravity acting on the polystyrene beads with diameters of 3, 10, and 20 μm, respectively. According to the potential energy curves in Fig. 8(a), the local maximum of the potential energy occurs very close to the position where the distance between the beads and the substrate is 1 nm or less under all conditions. In addition, the local maximum of the potential energy increases with the particle size. On the other hand, in Fig. 8(b), it can be seen that the maximum value of the attractive force is at a position where the distance between the beads and the substrate is relatively large (20 to 30 nm). Therefore, the adhesion behavior of the beads is considered to be caused by the local minimum existing in front of the electrical repulsion force peak. In addition, the local minimum value of the interaction force between the beads and the substrate also correlates with the particle size, similarly to the potential energy. From the above, it is considered that the increase in the adhesion rate due to the increase in particle size is significantly affected by the change in curvature at the interface of the particles. In addition, the local minimum of the interaction force based on DLVO theory is larger than the sedimentation force generated by gravity under all conditions. Therefore, it is considered difficult to remove non-specifically adsorbed beads by applying gravity within the particle size range used in this experiment. From the above, it is concluded that the influence of the gravitational potential of the beads within the particle size range tested is very limited, and the change in the interface due to the change in the particle size affects the adsorption behavior of the beads.

3.4 Evaluation of bead adhesion rate by Brownian motion analysis

Next, the correlation between the adhesion rates measured by Brownian motion analysis and by the gravity application method was investigated. The changes in the adhesion rate of 3 μm PS-COOH with the ionic strength of the solvent changed from 1.8 to 40 mM were examined and compared with the results obtained by both Brownian motion analysis and the gravity application method. The same experiment was performed three times, and the variation among the experiments was also investigated. The results are shown in Fig. 9. Results similar to those in

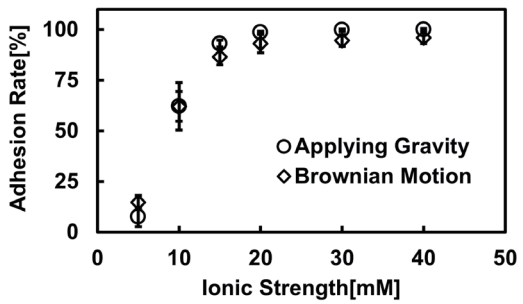

Fig. 9. Comparison of gravity application method and Brownian motion analysis method.

Sects. 3.2 and 3.3 were obtained by measuring the adhesion rate by the gravity application method, and the adhesion rate of the beads could be evaluated by the separation operation in which gravity acted on the beads. As shown in Fig. 9, the results obtained by Brownian motion analysis and the gravity application method have the same trend, with both sets of results showing a correlation between the ionic strength and the bead adhesion rate. These results show that it is possible to discriminate the adhering and non-adhering states of beads by Brownian motion analysis without a separation operation. On the other hand, at a high ionic strength, the adhesion rate in the gravity application method was higher than that obtained by Brownian motion analysis. This shows that a small number of particles that have undergone non-specific adsorption with the substrate exhibit slight Brownian motion on the substrate. Therefore, it is shown that in the non-specific adsorption of beads, there are both beads with sufficiently strong adsorption to constrain Brownian motion and those with weak adsorption, allowing slight Brownian motion. Future investigation is necessary to examine the cause of these differences in adsorption behavior.

3.5 Effect of interaction time on bead adhesion rate

Next, the results of analyzing the time change of the adhesion rate by observing Brownian motion by interacting the amino-group-modified microbeads and the carboxyl-group-modified microbeads with the slide glass are shown in Figs. 10(a) and 10(b). Figure 10(a) shows that the beads settle due to gravity and the number of beads on the substrate surface increases with time. Figure 10(b) shows the time change of the adhesion rate of each particle. A HEPES solution with an ionic strength of 1.8 mM and a pH of 6.9 was used as the dispersion medium. In addition, for the equation in Fig. 10(b), the slope corresponds to the time variation of the bead adhesion rate, and it is considered that the intercept shows the bead adhesion rate without the time variation. As shown in Fig. 10(b), the adhesion rate is highest from 0 to 10 min. This is considered to be due to noise caused by the erroneous detection of dust and other particles in the image analysis. Since the noise due to erroneous detection is small, when the total number of beads is large, the effect on the adhesion rate is small. However, when the beads were added to the reaction chamber,

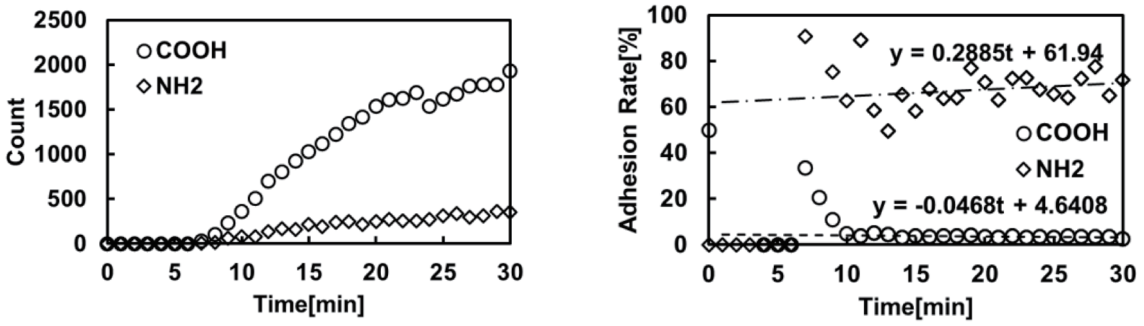

(a) (b)

Fig. 10. (Color online) Observation of time changes in bead adhesion rate. (a) Time change in total number of beads. (b) Time change in bead adhesion rate.

some erroneous detection noise was present, and it is considered that the adhesion rate increased. As shown in Fig. 10(b), the amino-group-modified beads have a higher adhesion rate than the carboxyl-group-modified beads. This is consistent with the fact that the surface potential of the beads is close to neutral, as can be seen from the measured zeta potential. Furthermore, in the carboxyl-group-modified beads, the total number of beads tended to increase monotonically with time, whereas the adhesion rate was almost constant. This means that the adhesion or non-adhesion of beads is determined at the time when the beads approach the substrate, and the transition between adhesion and non-adhesion is unlikely to occur with time. On the other hand, the adhesion rate of the amino-group-modified beads tended to increase slightly with time. The zeta potential of these beads is slightly shifted in the neutral direction due to the amino groups on the bead surface, and the repulsive potential due to the electrostatic interaction was small. Therefore, the time change of the adhesion rate is considered to be because Brownian motion in the amino-group-modified beads moves to the adsorption site on the substrate surface and the beads transition from the non-adhering state to the adhering state. That is, the adhesion of beads is determined by a slight difference in the charge distribution and the position on the substrate approached by the beads.

It was confirmed with good reproducibility that the adhesion rate of the amino-group-modified beads increased with time. However, the range of the transition of the adhesive force was found to gradually change with increasing number of days from the preparation of the bead suspension. It is considered that the surface potential of the amino-group-modified beads is shifted in the negative direction, and further research is required to establish the reason.

3.6 Bead-based bioanalytical system design strategy

In this paper, we propose bead separation by gravity and adhesion rate analysis by Brownian motion. In bead separation by applying gravity, the non-specific adhesion of beads is distinguished by using the sedimentation force obtained by subtracting the buoyancy from the gravity acting on the beads as the threshold value for specific/non-specific binding. On the other hand, in the adhesion rate analysis using Brownian motion, non-specific adhesion of beads is detected by the inhibition of Brownian motion by the attractive force acting between the beads and the substrate. It has been shown that the adhesion obtained from these methods can be explained on the basis of DLVO theory. Therefore, the proposed particle adhesion analysis method provides useful knowledge for the development of bead-based bioanalysis systems. This section summarizes the design strategy of a bead-based bioassay system based on the above findings. Clearly physical adsorption occurred when a dispersion medium with high ionic strength such as DPBS was used. Adjusting the ionic strength of the bead dispersion medium is effective for reducing such adsorption. Furthermore, even for the same ionic strength of the dispersion medium, the adhesion rate greatly varies with the particle size. In the experiment, non-specific bead adhesion was hardly observed when a solvent having an ionic strength of 2 mM or less was used with polystyrene microbeads having a diameter of 3 μm. Therefore, it was confirmed that the above conditions are suitable for bead-based bioassay. On the other hand, from Brownian motion analysis, when a sufficient potential barrier is present, it is stably held by

the potential barrier even for an interaction time scale of several hours, and no significant adhesion occurs. In addition, this is longer than the incubation time of a general immune response. However, we suggest that it is necessary to study an appropriate immobilization method using a molecular spacer or a similar approach when the force balance distance is larger than the size of a biomolecule such as an antibody. For bead-based bioassay, it is necessary to study the bead–substrate interaction with the biomolecule modified as a practical consideration. Therefore, it is considered necessary to design an interface that maintains the potential barrier by controlling the antibody modification density and suppresses the adhesion of non-specific beads.

4. Conclusions

In this paper, we proposed an adhesion analysis technique by applying gravity and image analysis as a simple analysis method for analyzing the non-specific adsorption mechanism of beads in bead-based bioanalysis. Brownian motion analysis can identify the adhering/non-adhering state of beads, similar to the gravity application method. Furthermore, it was confirmed that these methods provide knowledge consistent with DLVO theory in analyzing the non-specific adhesion of fine particles. We successfully investigated the effects of important parameters such as the ionic strength, bead diameter, and interaction time in bioanalysis on the adhesion rate of particles. It is considered that a system design strategy based on systematic analysis by the proposed method can be established, even for a more complicated system in which biomolecules and polymers are introduced on a particle surface.

Acknowledgments

This work was supported by JSPS KAKENHI Grant Numbers 17H04746 and 15K12505.

References

1 M. Asal, Ö. Özen, M. Şahinler, and İ. Polatoğlu: Sensors **18** (2018) 1924. https://doi.org/10.3390/s18061924
2 D. S. Skelley, L. P. Brown, and P. K. Besch: Clin. Chem. **19** (1973) 146. https://doi.org/10.1093/clinchem/19.2.146
3 R. S. Yalow and S. A. Berson: Gastroenerology **58** (1970) 1. https://doi.org/10.1016/S0016-5085(70)80086-5
4 S. J. Goldsmith: Seminars in Nuclear Medicine **5** (1975) 125. https://doi.org/10.1016/S0001-2998(75)80028-6
5 J. Sun, T. Hu, C. Chen, D. Zhao, F. Yang, and X. Yang: Anal. Chem. **88** (2016) 9789. https://doi.org/10.1021/acs.analchem.6b02847
6 J. M. Hicks: Human Pathol. **15** (1984) 112. https://doi.org/10.1016/S0046-8177(84)80049-0
7 J. Briggs, V. B. Elings, D. F. Nicoli: Science **212** (1981) 1266. https://doi.org/10.1126/science.7015511
8 S. D. Gan and K. R. Patel: J. Invest. Dermatol. **133** (2013) e12. https://doi.org/10.1038/jid.2013.287
9 R. M. Lequin: Clin. Chem. **51** (2005) 2415. https://doi.org/10.1373/clinchem.2005.051532
10 M. F. Clark and A. N. Adams: J. Gen. Virol. **34** (1977) 475. https://doi.org/10.1099/0022-1317-34-3-475
11 D. Castro, D. Conchouso, R. Kodzius, A. Arevalo, and I. G. Foulds: Genes **9** (2018) 281. https://doi.org/10.3390/genes9060281
12 R. L. Edelstein, C. R. Tamanaha, P. E. Sheehan, M. M. Miller, D. R. Baselt, L. J. Whitman, and R. J. Colton: Biosens. Bioelectron. **14** (2000) 805. https://doi.org/10.1016/S0956-5663(99)00054-8
13 W. Cui, M. He, L. Mu, Z. Lin, Y. Wang, W. Pang, M. Reed, and X. Duan: ACS Sens. **3** (2018) 432. https://doi.org/10.1021/acssensors.7b00866
14 D. R. Basel, G. U. Lee, M. Natesan, S. W. Metzger, P. E. Sheehan, and R. J. Colton: Biosens. Bioelectron. **13** (1998) 731. https://doi.org/10.1016/S0956-5663(98)00037-2

15 M. Otake and Y. Ukita: Jpn. J. Appl. Phys. **58** (2019) SIIC03. https://doi.org/10.7567/1347-4065/ab1b5e
16 M. Otake and Y. Ukita: Anal. Sci. **35** (2019) 1123. https://doi.org/10.2116/analsci.19P137
17 Jessanne Y. Lichtenberg, Yue Ling, and Seunghyun Kim: Sensors **19** (2019) 2488. https://doi.org/10.3390/s19112488
18 S. Upadhyayula, T. Quinata, S. Bishop, S. Gupta, N. R. Johnson, B. Bahmani, K. Bozhilov, J. Stubbs, P. Jreij, P. Nallagatla, and V. I. Vullev: Langmuir **28** (2012) 5059. https://doi.org/10.1021/la300545v
19 T. Pochechueva, A. Chinarev, N. Bovin, A. Fediera, F. Jacob, and V. H. Schwarz: J. Immunol. Methods **412** (2014) 42. https://doi.org/10.1016/j.jim.2014.06.015
20 J. V. Jokerst, T. Lobovkina, R. N. Zare, and S. S. Gambhir: Nanomedicine **6** (2011) 715. https://doi.org/10.2217/nnm.11.19
21 C. A. Schneider, W. S. Rasband, and K. W. Eliceiri: Nat. Methods **9** (2012) 671. https://doi.org/10.1038/nmeth.2089
22 J. Schindelin, I. A. Carreras, E. Frise, V. Kaynig, M. Longair, T. Pietzsch, S. Preibisch, C. Rueden, S. Saalfeld, B. Schmid, J. Y. Tinevez, D. J. White, V. Hartenstein, K. Eliceiri, P. Tomancak, and A. Cardona: Nat. Methods **9** (2012) 676. https://doi.org/10.1038/nmeth.2019
23 E. J. W. Verwey and J. Th. G. Overbeek: Theory of the stability of lyophobic colloids (Elsevier, Amsterdam, 1948) pp. 135–182.
24 E. Stellwagen, J. D. Prantner, and N. C. Stellwagen: Anal. Biochem. **373** (2008) 407. https://dx.doi.org/10.1016%2Fj.ab.2007.10.038